EXPERIMENTAL DETAILS

AC powder (Norit SX Ultra from Sigma Aldrich Corp.) based electrodes were prepared without binder using 5% CNTs by weight [6]—through a vacuum filtration based process. Briefly, 5 mg of CNTs were sonicated for 30 min in 100 mL of benzyl alcohol with a Core-Palmer 8891 sonication instrument. Subsequently, 100 mg of AC powder was added to the solution which was then sonicated for 1 hour. The solution was subject to vacuum filtration, and the filtrate washed with ethyl alcohol, and then deionized water. The electrode was then dried at 100°C for 12 hours. Subsequently, ~1 cm^2 pieces of the electrodes (comprising the AC as well as the filter paper – which served as the separator) were used for electrochemical experimentation.

The electrodes were ion irradiated with argon plasma (in a Trion Reactive Ion Etching: RIE, chamber). Argon plasma power was set to 100W, 200W, 300W, and 500W, with an estimated ion density of ~ 10^{11} /cm^3. Subsequently, a series of techniques, e.g., cyclic voltammetry (CV), Constant Current Charge/Discharge (CCCD), and Electrical Impedance Spectroscopy (EIS) were performed on the electrodes using a Gamry PCI4 based potentiostat. A set of two electrodes were placed in an assembled testing apparatus (MTI Corp.): see Figure 1. An acetonitrile electrolyte, with dissolved Tetrabutyl-ammonium hexafluorophosphate ($TBAPF_6$) at 0.3 M, was employed. Surface area measurements via BET (Brunauer-Emmett-Teller) methods were performed on the untreated AC electrodes to confirm high internal surface area. While the specific surface area (SSA) of ~1000 m^2/g was obtained for the pristine AC powder, and the AC/CNT matrix powder, the projected area (~1 cm^2) was used for the purpose of area normalization in this paper.

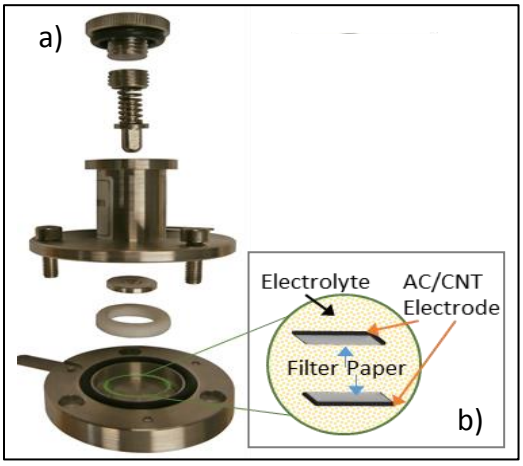

Figure 1. An electrochemical split test cell. (a) A disassembled cell (b) a detailed diagram of the electrodes and electrolyte within the test chamber.

RESULTS AND DISCUSSION

Cyclic Voltammetry (CV)

CV considers the variation of the electrical current in the AC electrodes as a function of applied voltage, with the area enclosed by the resulting characteristics proportional to the power that can be obtained from an EC. In our experiments, the CV was conducted at various voltage scan rates (v) ranging from 10 mV/s to 500 mV/s. A more rectangular voltammogram is generally indicative of greater capacitive double layer contribution, with deviations due to redox-associated contributions. The capacitance was estimated from the voltammogram through [7]:

$$C_{dl} = \frac{P(t)}{v \cdot V(t)} = \frac{\int_{V_1}^{V_2} i dV}{2 \cdot v \cdot V(t)} \dots\dots\dots (1) \qquad C_{net} = \frac{2C_{dl}}{A_{proj}} = \frac{\int_{V_1}^{V_2} i dV}{v \cdot V(t)} \dots\dots\dots (2)$$

Here, $P(t)$ is the power of the capacitor, V_1 and V_2 are the initial and final voltage limits, respectively, $V(t)$ is the time varying voltage, and A_{proj} is the projected area of the electrode.

Since the two AC electrodes in the cell are in series, the capacitance of electrode would be twice that of the calculated value.

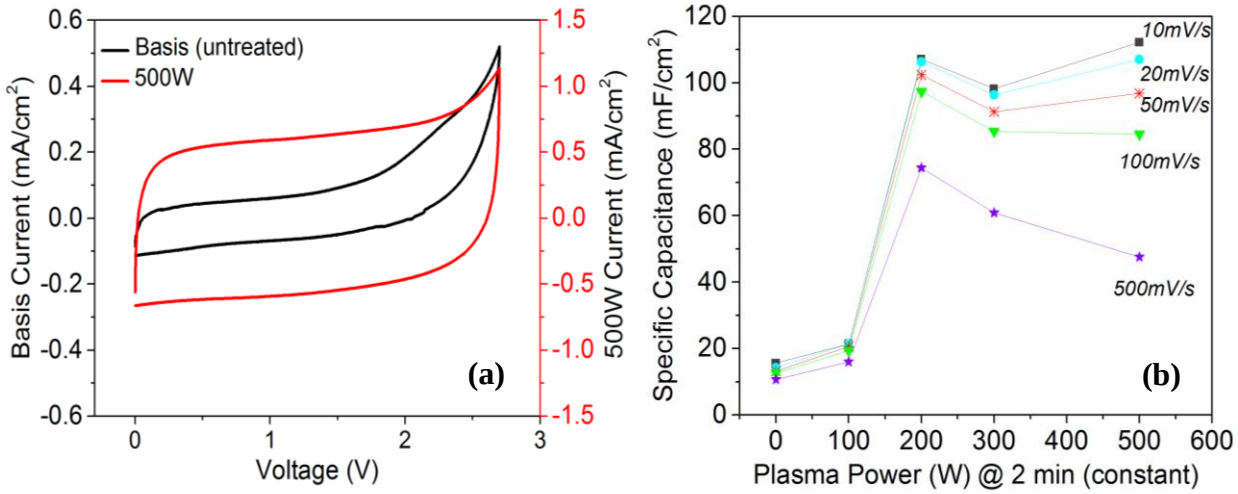

Figure 2. Cyclic Voltammetry: AC electrodes were tested at scan rates in the range of 10 mV/s to 500 mV/s, over at least five cycles (averaged values are indicated) in the voltage window of 0 – 2.7 V. (a) the control pair of electrodes (*not* subject to plasma processing) and electrodes, subject to 500 W of argon ion plasma processing at 10 mV/s. (b) Capacitance as a function of Ar^+ plasma power.

It was seen that the CV scans on the 500W (Argon plasma power) treated electrodes were more rectangular shaped, especially at lower scan rates (see Figure 2a). The sharp increase of the curve past ~2V is possibly due to a parasitic redox couple, e.g., due to absorbed ionic species. At 10 mV/s, the capacitance from the CV measurement was seen to increase from 15.6 mF/cm^2 to 112 mF/cm^2 (see Figure 2b). The increase was ascribed to the plasma processing, which would have introduced additional charged defects that add to the double layer capacitance, evidenced by the smaller redox contribution of the 500W curve. The capacitance of the activated carbons generally increases with plasma processing power due to the hypothesized addition of additional plasma generated charges. However, there is a relative saturation of the capacitance increase at/beyond 200 W with a lower rate capability/larger variation with scan rate at larger power, *e.g.*, at 500 W. One plausible explanation for the wider variation of capacitance is that the higher penetration depths corresponding to larger plasma power may damage the surface of carbon, leading to increased resistive effects.

Constant Current Charge/Discharge (CCCD)

. Further corroboration of the capacitance increase was obtained. CCCD based testing is often used to characterize the performance of ECs under the application of a direct current. The EC is charged/discharged at a constant current and the ratio of the applied current to the consequent rate of change of voltage would be a gauge of the capacitance value (Eqn. 3) and would be estimated through [7,8]:

$$C_{dl} = \frac{I}{dV/dt} = \frac{I \cdot (t_2 - t_1)}{\left(\frac{3}{4}V_{max} - \frac{1}{4}V_{max}\right)} \ldots\ldots\ldots (3)$$

I is the constant current input to the EC, *dV/dt* is the slope of the discharge curve and t_1 and t_2 correspond to the time needed to achieve the voltages to the ¾ and the ¼ of the maximum level. The voltage level definitions were in accordance with the prescriptions of a best-practice method [8]. The applied current (*I*) was chosen so as to yield *dV/dt* close to ~ 10 mV/s. Consequently, the estimated capacitance was compared to that obtained from CV at 10 mV/s (see Table I).

Table I. AC capacitive increase via plasma processing, obtained through three different methods

	Basis *(mF/cm^2)*	**500W** *(mF/cm^2)*	**Factor of Increase**
CV	15.6	112	7.2
CCD	6.6	39.6	6.0
EIS	4.3	33.6	7.8

As seen from Figure 3, the shape of the voltage-time curve is nonlinear indicating that a ratio based definition may not be easy to use due to the ambiguity at which point to consider the *dV/dt*. Again, we see the condition that not all of the current contributes to double-layer charging, and C_{dl}, as there may be redox couple contributions [9]. Such characteristics may indicate a variable and increasing capacitance, per the definition of Eqn. (3), and may relate to the porous characteristics of the AC, i.e., with increasing time, more of the pores may participate enhancing the recorded capacitance.

While it was observed that the CCCD based capacitance values were lower than those determined through CV, the enhancement due to plasma processing is close to that estimated earlier and clearly indicates the utility of our methodology. Moreover, the obtained slopes of the control and plasma processed AC electrodes (at 7.75 mV/s and 16.5 mV/s) differ from the 10 mV/s used for the capacitance determined through CV.

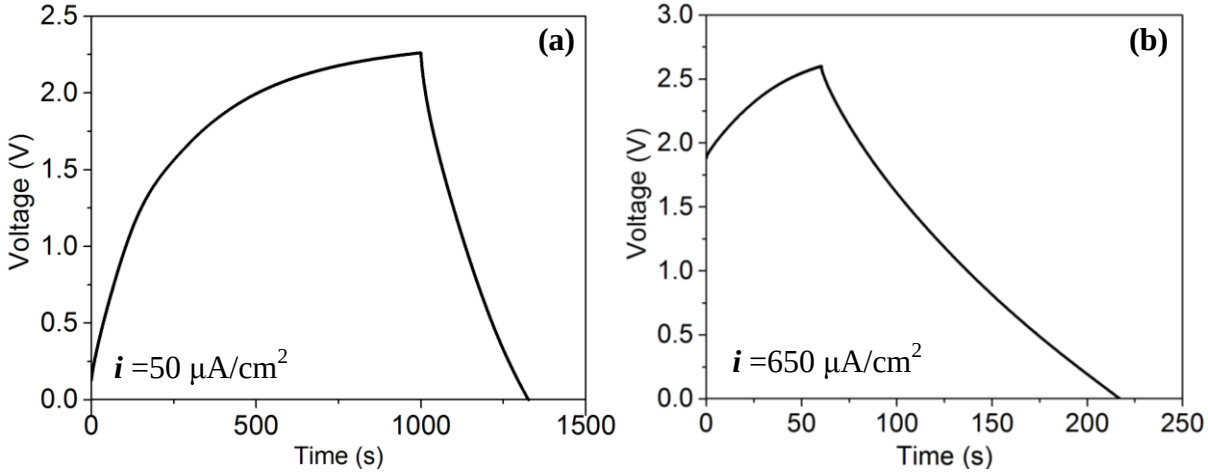

Figure 3. Constant current charge/discharge (CCCD) testing was performed on (a) the untreated and (b) plasma treated AC electrodes. The IR drop of the electrodes were ~ 385 mΩ and ~ 460 mΩ, respectively. V_{max} for both curves was set to 2.6 V.

Electrical Impedance Spectroscopy (EIS)

EIS is an alternating current based technique, where the impedance of an EC is determined as a function of the current frequency. Both the solution and the charge transfer resistance as well as the double layer capacitance may be estimated. The general characteristics of the plots (Figure 4), suggest an impedance model of the AC electrodes in terms of a Randles circuit, with kinetic (charge transfer) limitations at high frequencies and diffusion (mass transfer) limitations at lower frequencies.

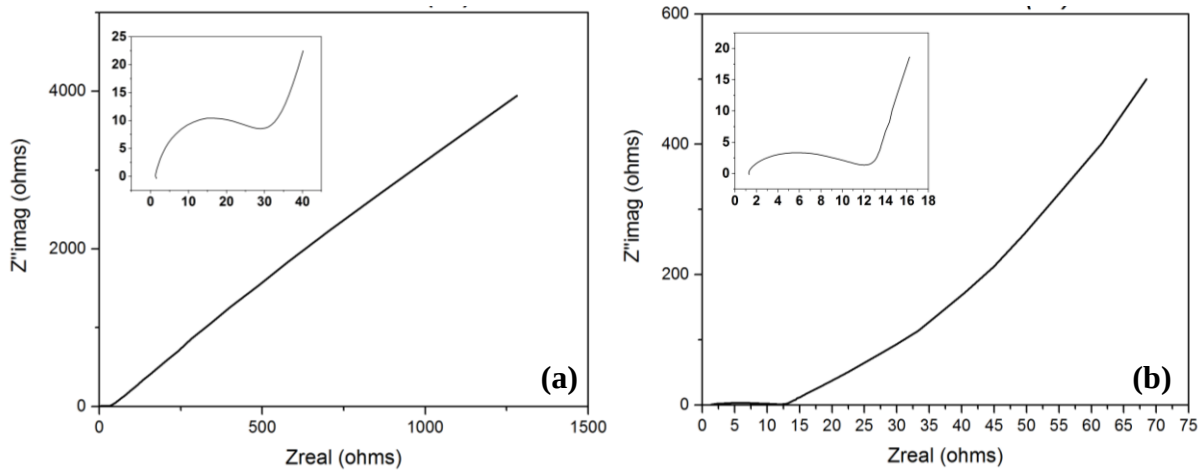

Figure 4. EIS (at 1V, in the frequency range of 10 mHz to 300 kHz). The inset to the graphs indicates the high frequency region of the graphs, with a solution resistance (R_s) of ~ 1 Ω. and a charge transfer resistance (R_{ct}) of ~30 Ω and ~9 Ω, for (a) the basis electrodes and (b) the 500 W plasma processed AC electrodes, respectively.

The R_{ct} and capacitance values were estimated from [8,9]:

$$R_{ct} = 2 \cdot \left(Z_{peak} - R_s\right) \dots\dots\dots (4) \qquad Z''_{imag} = \frac{-1}{\omega \cdot C_{dl}} \dots\dots\dots (5)$$

The R_{ct} is the charge transfer resistance, Z_{peak} is the real part of the impedance corresponding to the height of the abscissa, R_s is the ohmic solution resistance, and ω (= $2\pi f$) is the angular frequency, integral to the imaginary part of the impedance, Z''_{imag}. The R_{ct} seems to be smaller for the plasma power processed AC electrodes, indicating higher exchange current densities and possible redox reactions at the charged defect sites (introduced due to the plasma processing)[9]. Such deviations from pure double layer characteristics are also evident in the CV (Figure 2a) and the CCCD (Figure 3a) scans. The maximum capacitance (estimated at 10 mHz), is indicated in Table I. The lowest frequency should be the most accurate since it will have allowed the electrolyte significant time to access the porous structure of the electrodes. While plasma processed AC electrodes show close to eight-fold enhanced capacitance, the discrepancy with the absolute values from the CV and the EIS may be due to non-comparable conditions of testing.

CONCLUSIONS

We have shown for the first time, plasma processing based capacitance enhancement on relatively large scale AC based electrodes (~120 microns thick). A six-eight fold increase of the capacitance is significant and would have a large impact in enhancing the energy density of electrochemical capacitors. While such enhancement was evidenced through three independent and standard electrochemical techniques, the specific values of the capacitance differ, possibly due to non-comparable testing conditions. Future work will focus on understanding such discrepancies, delineating the contributing electrochemical processes and characteristics, all of which would enable a comprehensive model for high energy density electrochemical capacitors.

ACKNOWLEDGEMENTS

We would like to thank the Nano3 Fabrication lab at UCSD. We appreciate the help of Dr. Seth Cohen and Dr. Zhenjie Zhang in BET surface measurements and calculations.

REFERENCES

1. Chmiola, J., Yushin, G., Gogotsi, Y., Portet, C., Simon, P., & Taberna, P. L. (2006). Anomalous increase in carbon capacitance at pore sizes less than 1 nanometer. *Science, 313*(5794), 1760-1763.
2. Karakaya, M., Zhu, J., Raghavendra, A. J., Podila, R., Parler Jr, S. G., Kaplan, J. P., & Rao, A. M. (2014). Roll-to-roll production of spray coated N-doped carbon nanotube electrodes for supercapacitors. *Applied Physics Letters,105*(26), 263103.
3. Okajima, K., Ohta, K., & Sudoh, M. (2005). Capacitance behavior of activated carbon fibers with oxygen-plasma treatment. *Electrochimica Acta, 50*(11), 2227-2231.
4. Hoefer, M., & Bandaru, P. (2013). Electrochemical Characteristics of Closely Spaced Defect Tuned Carbon Nanotube Arrays. *Journal of The Electrochemical Society, 160*(6), H360-H367.
5. Narayanan, R., Yamada, H., Karakaya, M., Podila, R., Rao, A. M., & Bandaru, P. R. (2015). Modulation of the electrostatic and quantum capacitances of few layered graphenes through plasma processing. *Nano letters*. DOI: 10.1021/acs.nanolett.5b00055
6. Xu, G., Zheng, C., Zhang, Q., Huang, J., Zhao, M., Nie, J., ... & Wei, F. (2011). Binder-free activated carbon/carbon nanotube paper electrodes for use in supercapacitors. *Nano Research, 4*(9), 870-881.
7. Stoller, M. D., & Ruoff, R. S. (2010). Best practice methods for determining an electrode material's performance for ultracapacitors. *Energy & Environmental Science, 3*(9), 1294-1301.
8. Conway, B. E. (1999). Electrochemical supercapacitors. 53 – 57, 486 – 496.
9. Bard, A. J., & Faulkner, L. R. (2001). Electrochemical methods: principles and applications. *Electrochemical Methods: Principles and Applications*. 386 – 428.